This is a post-peer-review, pre-copyedit version of an article published in NATURE PLANTS. The final authenticated version is available online at: http://dx.doi.org/10.1038/nplants.2016.131

LHCII can substitute for LHCI as an antenna for photosystem I but with reduced light-harvesting capacity

Mauro Bressan[1], Luca Dall'Osto[1], Ilaria Bargigia[2], Marcelo J. P. Alcocer[2,3], Daniele Viola[3], Giulio Cerullo[3], Cosimo D'Andrea[2,3], Roberto Bassi[1]* and Matteo Ballottari[1]

Light-harvesting complexes (LHCs) are major constituents of the antenna systems in higher plant photosystems. Four Lhca subunits are tightly bound to the photosystem I (PSI) core complex, forming its outer antenna moiety called LHCI. The Arabidopsis thaliana mutant ΔLhca lacks all Lhca1–4 subunits and compensates for its decreased antenna size by binding LHCII trimers, the main constituent of the photosystem II antenna system, to PSI. In this work we have investigated the effect of LHCI/LHCII substitution by comparing the light harvesting and excitation energy transfer efficiency properties of PSI complexes isolated from ΔLhca mutants and from the wild type, as well as the consequences for plant growth. We show that the excitation energy transfer efficiency was not compromised by the substitution of LHCI with LHCII but a significant reduction in the absorption cross-section was observed. The absence of LHCI subunits in PSI thus significantly limits light harvesting, even on LHCII binding, inducing, as a consequence, a strong reduction in growth.

The conversion of light into chemical energy occurs in pigment–protein complexes, the photosystems. In eukaryotic photosynthetic organisms, two photosystems, namely PSI) and PSII, undergo light-driven charge separation. PSI and PSII bind chlorophyll (Chl) and carotenoid (Car) chromophores, whose spectroscopic properties are tuned by the protein environment. The initial reactions within PSI and PSII are catalysed by Chl a dimers, which absorb at 700 and 680 nm respectively. These dimers are served by a closely interacting array of Chl a and β-carotene pigments which are bound to plastid-encoded proteins in the so-called core complexes. More specifically, the PSI core (PSIc) complex comprises 95–98 Chls[1,2], but the PSII core complex binds fewer Chls (36). The optical absorption cross-section of both core complexes is enhanced by an outer antenna system composed of nuclear-encoded LHC subunits[3–6]. Higher plants evolved four LHC subunits (Lhca1–4) arranged in a half-moon structure adjacent to the PsaF/PsaJ subunits of the PSI core complex[1,2,7–9]. The PSIc/LHCI stoichiometry has been shown to be maintained at 1:4 irrespective of light growth conditions[10]. In contrast, the dimeric PSII core is encircled by a larger LHC antenna system composed of Lhcb1–6 subunits. These are organized into monomers (Lhcb4–6) and trimers (Lhcb1–3, also known as LHCII complexes), with the monomers located in between the core complex and the more peripheral trimers. Lhcb proteins can, however, migrate from PSII to PSI along the thylakoid membranes, depending on photosystem excitation[11–17]. When PSI is preferentially excited, plastoquinole (PQH_2) is oxidized and LHCII is almost exclusively associated to PSII (state 1). Upon preferential PSII excitation, however, PQH_2 undergoes over-reduction and triggers a threonine kinase activity which targets LHCII, freeing it from PSII grana and allowing diffusion to PSI (state 2)[16,18–21]. This transition bala-nces excitation energy pressure between the photosystems, restoring the plastoquinone/PQH_2 ratio. It is reversed by TAP38/PPH1 phosphatase on PQH_2 re-oxidation[22–24]. The interaction of LHCII with PSI was observed under several growth conditions as a consequence of acclimation to low or moderate light levels[10,20,25], and was observed even in the absence of LHCII phosphorylation[15]. Upon binding to PSI, LHCII trimers have been shown to efficiently transfer excitation energy to the PSI reaction centre[25–27]. PSI supercomplexes binding either LHCI or LHCII, or both, differ as to their spectra and the strength of the PSIc–LHC interactions. In this work we investigated whether LHCI and LHCII are functionally equivalent when bound to PSI. To this extent, we isolated a ΔLhca mutant of A. thaliana which lacks the Lhca1–4 subunits and accumulates PSI core complexes with LHCII bound, analysing plant growth, light-harvesting and excitation energy transfer properties of its PSI complexes compared to wild type.

Results

ΔLhca is a triple knockout mutant of Arabidopsis, lacking all four Lhca subunits of the PSI peripheral antenna system. ΔLhca plants were obtained by crossing homozygous T-DNA mutants carrying insertions in genes encoding Lhca2, Lhca3 and Lhca4. We identified single knockout homozygous plants koLhca2, koLhca3 and koLhca4 in T-DNA F5 seed pools by polymerase chain reaction (PCR) analysis of genomic DNA (see Methods section). The triple knockout mutant, hereafter referred to as ΔLhca,was obtained by crossing single mutants and screening of the progeny. RT–PCR showed that mRNAs encoding Lhca2–4 were absent in the triple mutant (Fig. 1a); transcription of Lhca1,onthe contrary, was similar in wild type and ΔLhca within experimental error (Supplementary Fig. 1). PSI antenna protein composition in triple mutant plants was investigated by one- and two-dimensional (2D) SDS–polyacrylamide gel electrophoresis (PAGE). Thylakoids from ΔLhca plants lacked Lhca2, Lhca3 and Lhca4 proteins (Fig. 1b); moreover, an additional band with higher molecular mass

[1]Dipartimento di Biotecnologie, Università di Verona, Strada Le Grazie 15, I-37134 Verona, Italy. [2]Centre for Nano Science and Technology @PoliMi, Istituto Italiano di Tecnologia, via Pascoli 70/3, 20133 Milan, Italy. [3]IFN-CNR, Department of Physics, Politecnico di Milano, Piazza Leonardo da Vinci 32, 20133 Milan, Italy. *e-mail: roberto.bassi@univr.it

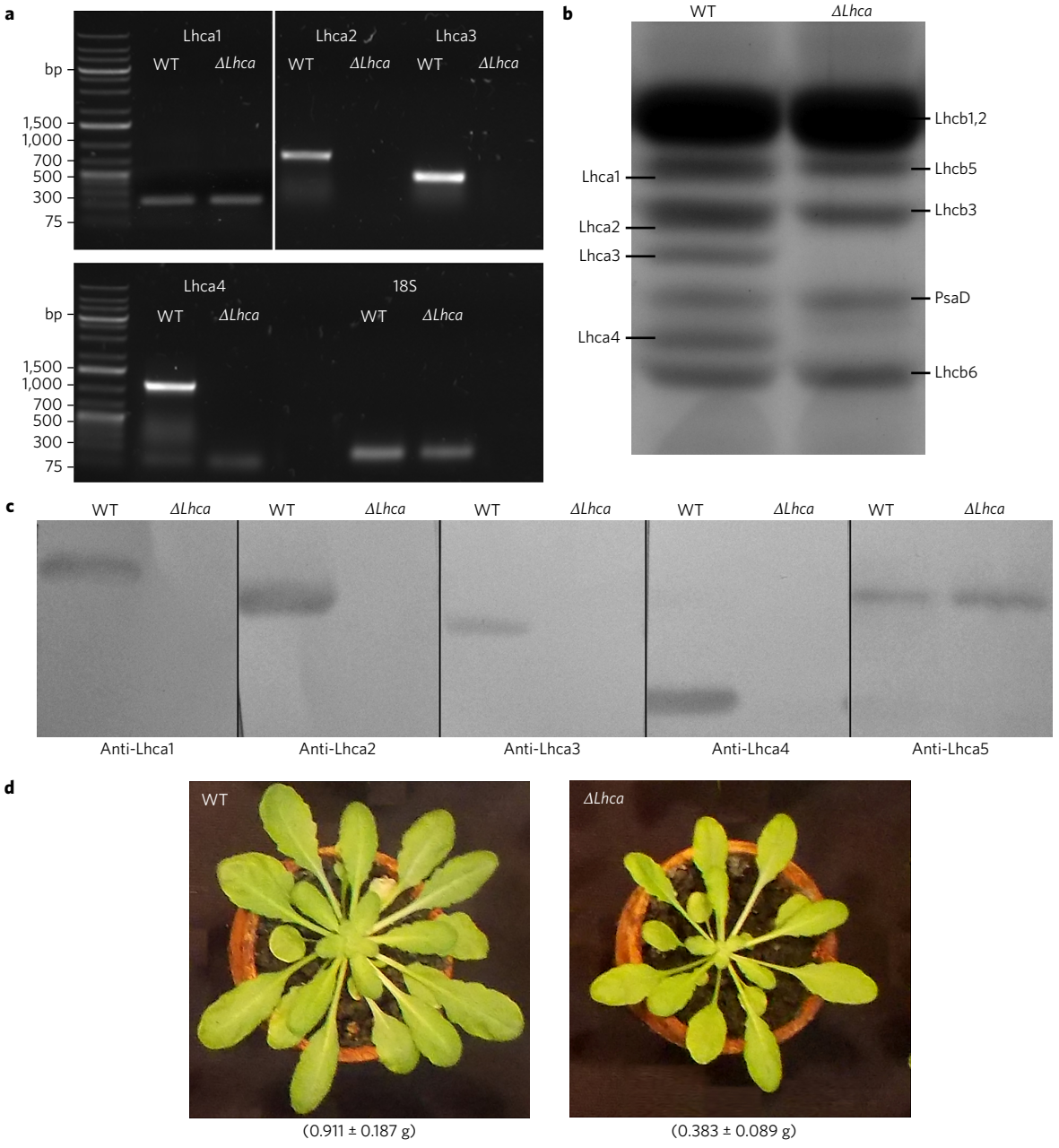

Figure 1 | Genetic and biochemical characterization of the *ΔLhca* mutant. a, RT–PCR verification of gene-specific transcripts. See Methods for sequences of the oligonucleotides used. For each gene, RNA extracted from wild-type (WT) and *ΔLhca* leaves was subjected to reverse transcription (top panel). Amplification of the housekeeping rRNA 18S from the same RNAs was used as loading control (bottom panel). bp, base pairs of molecular weight marker. Expected sizes of the amplicons: Lhca1, 752 bp; Lhca2, 751 bp; Lhca3, 487 bp; Lhca4, 1,049 bp and 18S, 149 bp. **b**, SDS–PAGE analysis of wild-type and *ΔLhca* thylakoid proteins. In each lane 15 μg of Chl was loaded. Selected apoprotein bands are marked. **c**, Immunoblot analysis. Thylakoid samples from the wild type and mutant were probed with antibodies specific for the different Lhca proteins. **d**, Phenotype of wild-type and mutant plants grown on soil for 4 weeks under constant, standard conditions (150 μmol photons m^{-2} s^{-1}, 23 °C, 8 h/16 h day/night). Fresh weight recovery is reported in grams, resulting from the average of five independent biological replicates. Standard deviation is reported.

than Lhca2 was also missing, which corresponded to Lhca1 as revealed by immunoblotting (Fig. 1c), implying that the *ΔLhca* mutant was devoid of all four Lhca subunits. This is consistent with Lhca4 being needed for the stable association of Lhca1 with the core[28,29]. Immunotitration showed that Lhca5 protein was present in higher amounts in *ΔLhca* (+50%) than in the wild type (Fig. 1c), consistent with a previous report on the Lhca4 single mutant[28]. To assess whether in *ΔLhca* Lhca5 was present in stoichiometric amounts with PSI, as in the case of Lhca1–Lhca4 proteins in the wild type, the 20–30 kDa region including LHC proteins was analysed by 2D SDS–PAGE. The separation allowed for identification of individual *Lhc* gene products as distinct spots (Supplementary Fig. 2), showing the complete lack of Lhca1–4 subunits in *ΔLhca*. Western blotting analysis on 2D maps localized Lhca5 in a region devoid of Coomassie-stained protein spots both in the wild type and in *ΔLhca* (Supplementary Fig. 2), implying Lhca5 was accumulated in sub-stoichiometric levels in both genotypes.

When grown in a climate chamber for 4 weeks under controlled conditions (150 μmol photons m^{-2} s^{-1}, 23 °C, 8 h/16 h, day/night), *ΔLhca* plants grew significantly less than wild-type plants with an almost 60% reduction in fresh weight (Fig. 1) indicating a significant reduced plant fitness in the absence of LHCI antenna proteins.

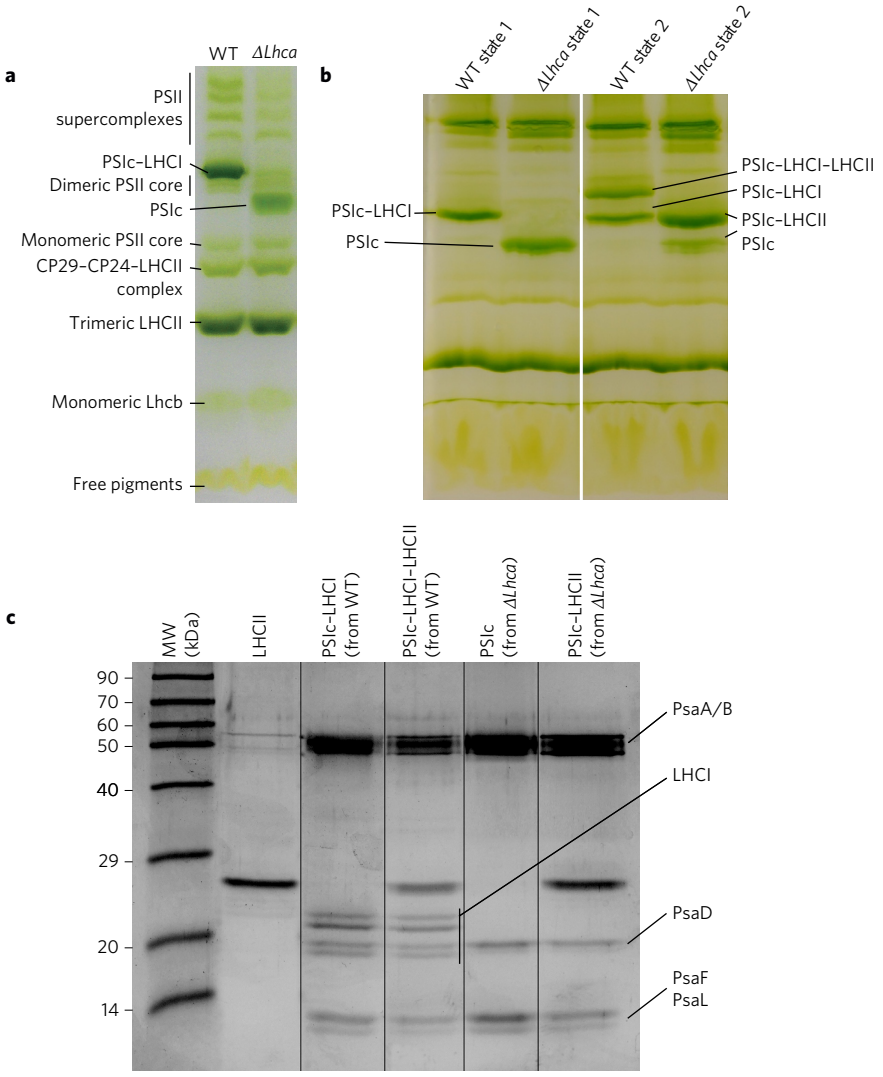

Figure 2 | Biochemical characterization of pigment–protein complexes. a, Thylakoid pigment–protein complexes were separated by non-denaturing Deriphat-PAGE on solubilization with 0.8% α-DM (n-Dodecyl α-D-maltoside). **b**, Native PAGE of thylakoid proteins isolated from wild-type and *ΔLhca* plants acclimated either to PSI or PSII light for 45 min before membrane isolation. A PSIc–LHCI–LHCII supercomplex is visible only in wild-type leaves treated with PSII light (state 2), whereas in the corresponding mutant sample a complex with higher apparent mass than PSI core represents the PSIc–LHCII supercomplex. These complexes are absent in samples from leaves treated with PSI light (state 1). **c**, SDS–PAGE of LHCII, PSIc, PSIc–LHCI, PSIc–LHCII and PSIc–LHCI–LHCII complexes eluted from native PAGE. The main protein components of each fraction and the molecular mass (MW) in kDa are indicated.

Photosynthetic function was investigated in intact leaves by measuring both PSII and PSI activities. Maximal quantum efficiency of PSII (F_v/F_m) was slightly higher in *ΔLhca* vs. wild-type plants (Supplementary Table 1). The time required to reach two-thirds of the maximum Chl fluorescence rise ($t_{2/3}$) in 3-(3,4-dichlorophenyl)-1, 1-dimethylurea (DCMU)-treated leaves, a measure of the functional antenna size of PSII (ref. 30), was slightly but significantly lower in the mutant (Supplementary Table 1). The functional antenna size of PSI was estimated from the ratio of P700 oxidation in limiting vs. high light exposure, obtaining a reduced antenna size in the *ΔLhca* mutant, thus confirming that LHCI depletion did reduce the overall optical cross-section of PSI. *ΔLhca* plants grown under control light did not differ from wild-type plants for Chl content per leaf area. However, a significant increase in both Chl *a*/*b* and Car/Chl ratios was observed (Supplementary Table I).

Isolation of PSI supercomplexes. The organization of pigment-binding complexes was analysed by non-denaturing Clear Native PAGE[31] (Fig. 2), on solubilization of wild type and *ΔLhca* thylakoids with 0.8% dodecyl maltoside. Several green bands were resolved in the wild type: the PSII pigment–proteins migrated as multiple bands with different apparent masses, namely the PSII core and the antenna sub-complexes, including the Lhcb4–Lhcb6–LHCII-M complex, the trimeric LHCII and the monomeric LHCBs. Instead, the PSI supercomplex was found as a single major band in the middle section of the gel. Green bands, with apparent mass higher than PSI–LHCI, contained undissociated PSII supercomplexes with different LHCII complements[29]. Densitometric analysis of the green band profile showed very similar distribution of pigment–protein complexes of PSII, implying that the lack of LHCI polypeptides had no effects on the relative abundance of PSII subunits. The major difference detected was the lack of PSIc–LHCI supercomplex and the appearance of a green band with lower apparent mass containing the PSIc in *ΔLhca*. To fully identify these green complexes, green bands in the region of PSI were excised and further analysed: depletion of Lhca1–4 polypeptides and the presence of PSI subunits PsaA/PsaB and PsaD (Fig. 2) confirmed that *ΔLhca* plants only accumulated the PSI core moiety of the supercomplex. Wild-type and *ΔLhca* plants were then treated with either orange (650 nm) or far red (735 nm) light, thereby preferentially exciting

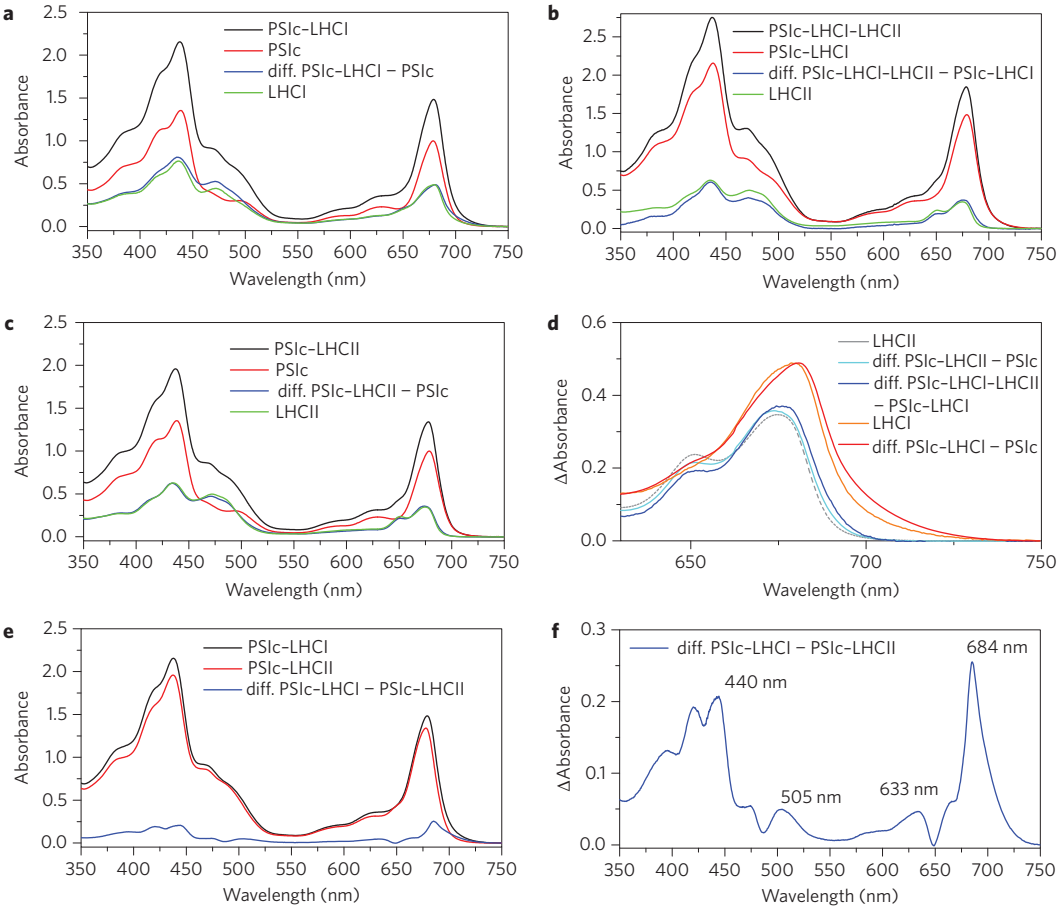

Figure 3 | Absorption spectra of PSI complexes. a–c, Spectra were normalized in order to have the same P700 content, as indicated in the Methods section. The difference (diff.) spectra reported in blue were obtained by subtracting PSIc from PSIc–LHCI (**a**), PSIc from PSIc–LHCII (**c**) or PSIc–LHCI from PSIc–LHCI–LHCII (**b**) and compared with LHCI (**a**) or LHCII (**b**,**c**), in both cases reported in green. **d**, The difference spectra in the Qy spectral region reported in **a**–**c** are compared with the absorption spectra of one LHCII trimer or one LHCI complex (four Lhca proteins). **e**, Comparison of PSIc–LHCI and PSIc–LHCII. The difference spectrum obtained by subtracting PSIc–LHCII from PSIc–LHCI is reported in **e** and in **f** in blue.

PSII or PSI (ref. 20). This results in LHCII phosphorylation and binding to PSI (state 2) or LHCII dephosphorylation and binding to PSII (state 1) respectively[13,20,32]. Purified thylakoid membranes were solubilized[26] and fractionated by Deriphat-PAGE[10], which allowed differential migration based on their apparent molecular size. The PSI supercomplexes of wild-type thylakoids from far-red-light-treated plants (state 1) migrated as a single major green band (Fig. 2)[29]. Fractionation of thylakoids from *ΔLhca* yielded similar results but the mobility of the PSI bands was higher, consistent with the lack of the LHCI moiety. It is important to notice that the abundance of the upper band in *ΔLhca* was strongly increased on treatment with orange light (state 2). PSI supercomplex bands were eluted from the acrylamide matrix and analysed. Western blot analysis (Supplementary Fig. 3) confirmed that the faster band in the wild type contained the PSIc–LHCI supercomplex and the slower band contained the PSIc–LHCI–LHCII supercomplex. The upper and lower bands from the *ΔLhca* sample consisted of PSIc and PSIc–LHCII complexes respectively. Even if Lhca5 was still present in *ΔLhca* thyalkoids, no traces of this subunit could be detected in any PSI complexes (Supplementary Fig. 3). The Chl *a*/*b* ratios of the isolated complexes are reported in Supplementary Table 2. The Chl *b* content per P700 was found to be highest in PSIc–LHCI–LHCII, decreasing in PSIc–LHCII and PSIc–LHCI in that order. This is in good agreement with the higher Chl *b* content in LHCII compared with LHCI (refs 1,2,33,34). As expected, only minor traces of Chl *b* were found in PSIc because of the absence of any LHC subunit in this complex. Interestingly, the Chl *a*/*b* ratios measured for PSIc–LHCII and PSIc–LHCI–LHCII were consistent with the addition of a single LHCII trimer per reaction centre, as previously reported[25,26].

Absorption properties of PSI supercomplexes. Differences in absorption cross-section of PSI on binding of LHCI and/or LHCII to PSIc were investigated by recording the absorption spectra of the PSIc, PSIc–LHCI, PSIc–LHCI–LHCII and PSIc–LHCII supercomplexes in the visible spectral region. The absorption spectra were normalized to be representative of PSI complexes with the same P700 content. This normalization was performed by taking into account the amount of Chl *a* and *b* bound by each complex (Supplementary Table 2), the ratio between the excitation coefficients of Chl *b*/*a* (0.7 as described in ref. 35), the Chls bound by PSIc (95–98 Chl *a*), LHCI (57–61) and LHCII (42), and finally the stoichiometry of PSIc/LHCI (1:4) and PSIc/LHCII (1:1)[1,2,7,8,33,34,36] (Fig. 3). Essentially the same absorption spectra and difference spectra were obtained by using the data reported by Mazor and coworkers[2], or Qin and coworkers[1]. The PSIc–LHCI minus PSIc difference spectrum peaked at 680 nm and had a low Chl *b* contribution (650 nm), closely mirroring the absorption spectrum of LHCI preparations[7] (Fig. 3a). Similarly, the PSIc–LHCI–LHCII minus PSIc–LHCI and PSIc–LHCII minus PSIc difference spectra closely resembled the absorption of trimeric LHCII, including a 676 nm peak and an enhanced 650 nm Chl *b* feature (Fig. 3b–d). It is worth noting that the difference spectra, which we tentatively attribute to PSI-connected

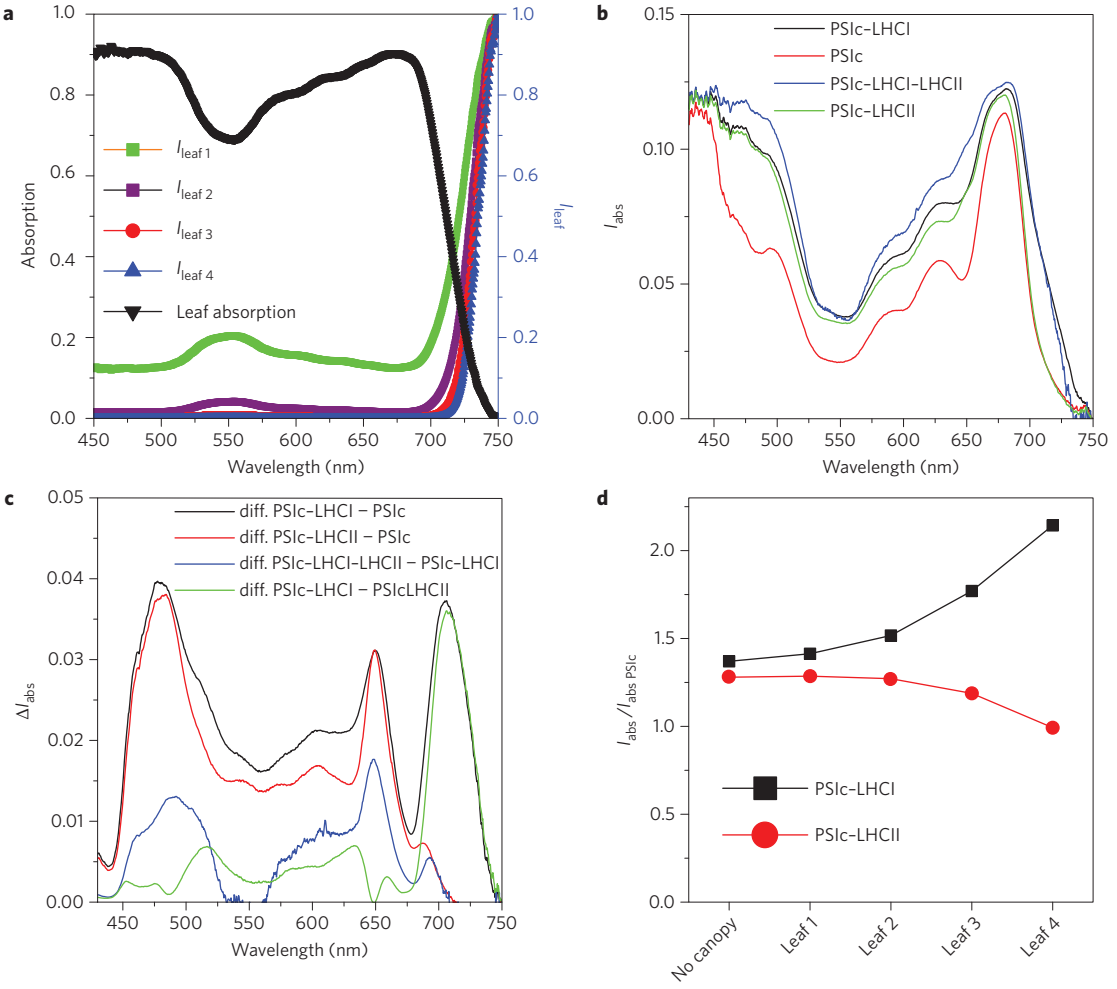

Figure 4 | Role of red-shifted absorption forms under canopy conditions. a, Leaf absorption in the visible region and wavelength dependence of the intensity of the light transmitted by four leaves (I_{leaf}) with each leaf shading the subsequent leaf. **b**, Light intensity absorbed (I_{abs}) by PSI complexes calculated considering the shading effect of one leaf. **c**, Differences in I_{abs} at the difference wavelengths calculated by subtracting the contribution of PSIc from PSIc–LHCI (black), from PSIc–LHCII (red), subtracting PSIc–LHCI from PSIc–LHCI–LHCII (blue) or subtracting PSIc–LHCII from PSIc–LHCI (green). **d**, Contribution of LHCI or LHCII to the capacity of PSIc to absorb light in different canopy conditions with shading of zero to four leaves. $I_{abs}/I_{abs\ PSIc}$ indicates the ratio between the light intensity absorbed by PSI-LHCI or PSI-LHCII and the light intensity absorbed by PSIc alone.

LHCII, closely matched the absorption spectrum of one LHCII trimer in both shape and amplitude based on the total number of Chls bound (24 Chl *a* and 18 Chl *b*) (Fig. 3d). We conclude that a single LHCII trimer was bound to either PSIc–LHCI or PSIc yielding PSIc–LHCI–LHCII and PSIc–LHCII supercomplexes respectively. When subtracting PSIc–LHCII from PSIc–LHCI (Fig. 3e), a positive difference spectrum was obtained throughout the visible range, as expected due to the different chlorophyll content bound by LHCI (57–61) and LHCII (42) (Fig. 3f). In particular, the difference spectrum was characterized by peaks at 420, 440, 633 and 684 nm, which are typical of Chl *a* bound to LHC proteins. Absorption forms above 700 nm were also detected, corresponding to the peculiar 'red forms' of LHCI (ref. 37). In addition, a small peak at 505 nm was evident, which is likely to be related to increased carotenoid content in LHCI compared with LHCII (13 vs. 12)[1,33]. To estimate the absorption cross-section in the different samples, the areas below the absorption spectra were computed and are reported in Supplementary Table 3; the values of each absorption cross-section were normalized to that of PSIc. The addition of LHCI or LHCII to PSIc caused an increase in cross-section of 67% and 51% respectively, and the absorption cross-section was more than doubled compared to PSIc when both LHCI and LHCII were bound to PSIc (PSIc–LHCI–LHCII supercomplex).

LHCI subunits allow PSI complexes to absorb light energy at wavelengths longer than 700 nm whose relative weight is enriched deeper in the canopy[38]. The absorption spectrum of a single leaf[39] was used to calculate the intensity of light transmitted through zero to four leaves (Fig. 4a), thus mimicking the intensity of the light absorbed by PSI complexes at different wavelengths (Fig. 4b) under canopy conditions. The presence of LHCI or LHCII bound to PSIc caused a strong difference in light absorption above 700 nm (Fig. 4c). When considering the cumulative effect of up to four leaves, the presence of LHCI becomes increasingly important, enhancing the amplitude of the absorption contribution by red forms at >700 nm by a factor of two or more compared with PSIc–LHCII (Fig. 4d).

Excitation energy transfer properties of PSI supercomplexes. The excitation energy transfer dynamics of LHCI vs. LHCII bound to PSIc were investigated using time-resolved fluorescence analysis. The kinetics of fluorescence decay on ultrafast femtosecond excitation of the Chls at either 440 or 475 nm were acquired by streak camera detection in the 500–900 nm range, as previously described[25,40–42]. The different excitation wavelengths were chosen to preferentially excite Chl *a* (440 nm) bound to both core complexes and antenna proteins, or Chl *b* (475 nm) bound to LHCI/LHCII only (Supplementary Table 4). The fraction of the

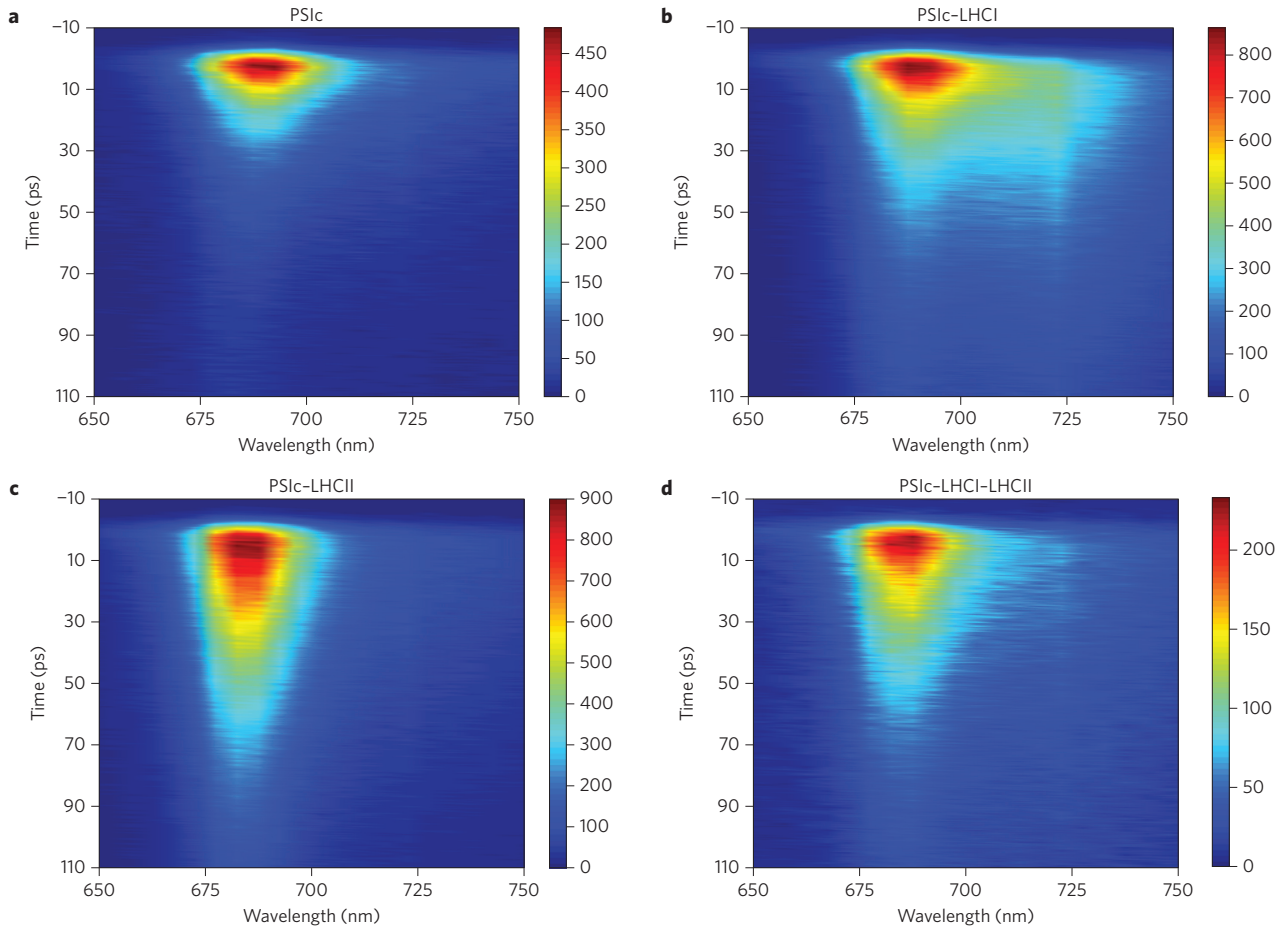

Figure 5 | Time-resolved fluorescence maps of different supercomplexes. a–d, Maps were obtained for the supercomplexes PSIc (**a**), PSIc–LHCI (**b**), PSIc–LHCII (**c**) and PSIc–LHCI–LHCII (**d**). Wavelength (nm) and time (ps) dependence of fluorescence emission are indicated on the *x* and *y* axes, respectively. The colour scale from blue to red represents fluorescence intensity from the lowest (blue) to the highest (red) intensity. The excitation wavelength was 475 nm.

PSI core excited at 440 or 475 nm in PSI–LHCI and PSI–LHCII was similar (65–70% on excitation at 440 nm and 38–39% on excitation at 475 nm), allowing a direct comparison of LHCI or LHCII contributions to the PSI complex excitation energy transfer (Supplementary Table 4). The fluorescence decay maps, as a function of wavelength and time, are reported in Fig. 5 (excitation at 475 nm) and Supplementary Fig. 5 (excitation at 440 nm). The main fluorescence peak was detected at ~688 nm in all the samples. In addition, a second peak was detected at ~725 nm, and can be attributed to the low energy emitting forms of LHCI (red forms) in both PSIc–LHCI and PSIc–LHCI–LHCII supercomplexes. To identify the decay components and their spectra (decay-associated spectra, DAS), the fluorescence decay kinetics in the 650–800 nm region were subjected to global analysis (Fig. 6 and Supplementary Fig. 7). Residues maps are reported for the different samples in Supplementary Figs 8 and 9 for excitation at 440 and 475 nm respectively. Fitting results at specific wavelengths are shown in Supplementary Fig. 10. Briefly, for each sample, the decay traces at the different wavelengths were fitted with multi-exponential functions, with the same decay constants being maintained through the entire spectral range. The amplitudes of the exponential functions, thus, form spectra associated to each decay constant (the DAS), as reported in Fig. 6. A fast DAS component with a lifetime between 3.8 and 8.8 ps was found to be present in all samples with positive/negative features. The presence of negative signal in the shortest DAS component of PSI was previously attributed to the excitation energy equilibration between bulk pigments and the low-energy forms[40–43]. Accordingly, the negative feature of the fastest DAS component was increased on preferential antenna excitation (475 nm) compared with 440 nm excitation, particularly in the presence of the red form containing LHCI. The predominant positive component in the shortest DAS, however, is mainly related to fluorescence decay rather than excitation energy transfer, likely to be from Chls in the core complex. In the case of PSIc, the main DAS obtained had a lifetime of 19 ps with a fluorescence emission peak at 692 nm. This 19–36.3 ps component was present in all complexes, and it has been previously associated with the bulk inner antenna Chls of PSIc (refs 40–43). Interestingly, in all samples with LHCII connected to a PSI core (PSIc–LHCI–LHCII and PSIc–LHCII), this DAS showed a slight blue shift to 687 nm and a significantly higher lifetime of 28–36 ps, independent of excitation wavelength. This suggests that the binding of LHCII to PSIc strongly contributed to the intermediate DAS (refs 25,26), most likely to be due to rapid equilibration of the energy absorbed by LHCII itself, with the strongest effect in the absence of LHCI (PSIc–LHCII complex). On excitation at 475 nm, the complexes containing LHC proteins (PSIc–LHCI, PSIc–LHCII and PSIc–LHCI–LHCII) were characterized by a major component with a relatively long lifetime between 58.3 and 68.2 ps, which was also detected on 440 nm excitation (61.3–72.8 ps), although with reduced amplitude (Supplementary Fig. 7). This long lifetime component has been previously associated with the outer LHCI antenna moiety in PSIc–LHCI as suggested by its dual emissions at 688 and 722 nm. In the case of the PSIc–LHCI–LHCII, the

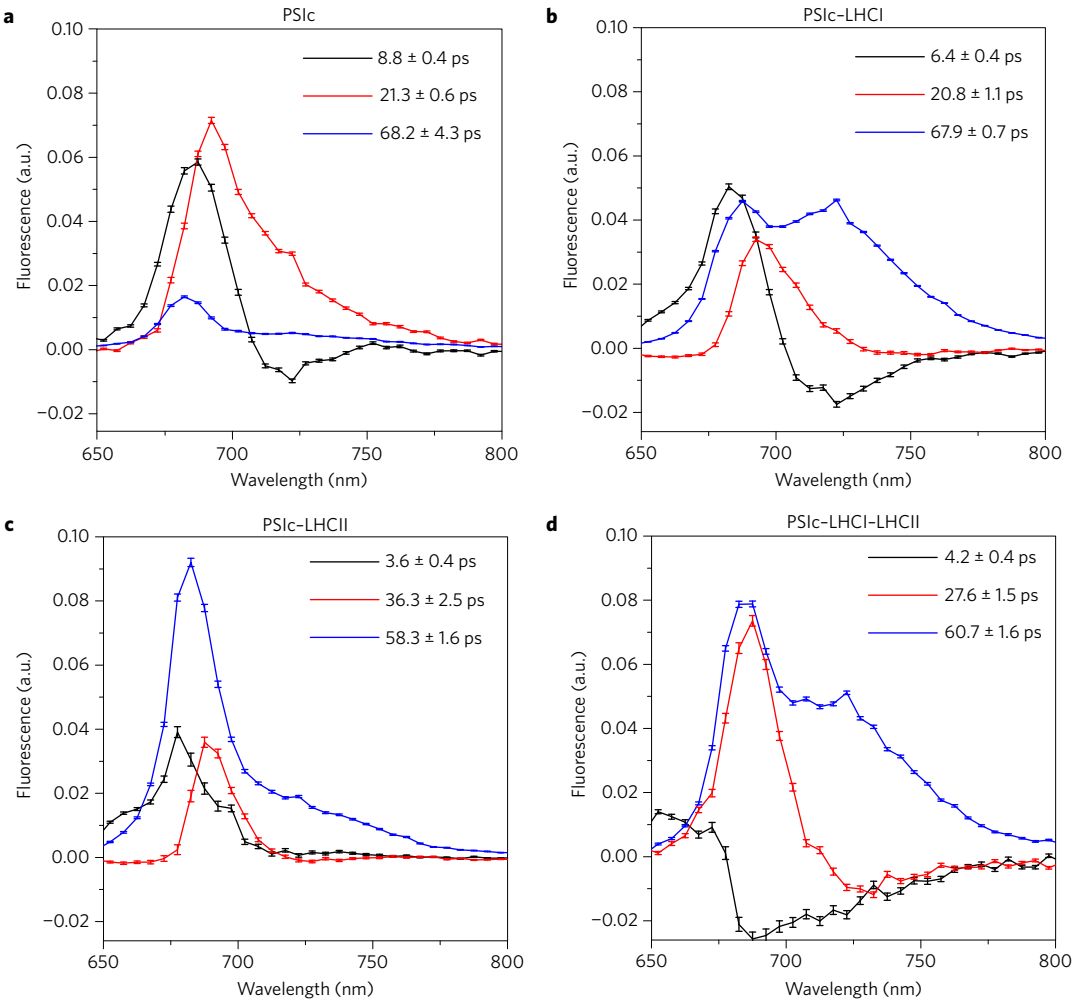

Figure 6 | Decay-associated spectra of PSI supercomplexes. a–d, The DAS were obtained for PSIc (**a**), PSIc–LHCI (**b**), PSIc–LHCII (**c**) and PSIc–LHCI–LHCII (**d**) from global analysis of the maps reported in Fig. 5. The excitation wavelength was 475 nm. The time constant associated with each DAS is indicated for each sample. Errors bars on DAS and time constants indicate the standard deviation.

weight of the 688 nm emission compared with the 722 nm emission was enhanced in the 60.7 ps DAS because of the LHCII contribution. In the case of the PSIc–LHCII, the long-lived DAS (58.3 ps) showed a reduced amplitude around 722 nm because of the lack of LHCI. Observation of this DAS component suggests that fast excitation energy transfer from LHCII to PSIc does occur, even in the absence of LHCI. A small 722 nm emission component with a 67.9 ps lifetime was detected in the PSIc decays, and was attributed to the red-shifted forms localized in the core complexes[40,42]. It is worth noting that this red-shifted component in PSIc can hardly be attributed to contamination from residual LHCI proteins, since this complex was purified from *ΔLhca* plants that lack the necessary encoding genes. To determine the influence of LHCI and LHCII on the excitation energy transfer to the PSI reaction centre, trapping times were estimated from the average fluorescence lifetimes of PSIc, PSIc–LHCI, PSIc–LHCII and PSIc–LHCI–LHCII. The results obtained are reported in Supplementary Table 5. The trapping time of PSIc was similar on 440 or 475 nm excitation, and binding of LHCI and/or LHCII significantly increased, in a similar way, the trapping time as a consequence of energy migration from the outer antenna proteins to the reaction centre. The calculation of the quantum efficiency of the different samples was performed based on previously reported methods[26,40,42] and yielded quantum yields higher than 98% in all samples. The spectral dependence of trapping time and quantum yield of PSI are shown in Fig. 7. An increased trapping time and reduced PSI quantum yield is evident in the 670–690 nm regions in the presence of LHCII or LHCI, and above 700 nm only in presence of LHCI. This result is consistent with the emission of LHCII at 680 nm, and of LHCI at both 680 and > 700 nm. Interestingly, at any emission wavelength, the quantum efficiency of PSI was always higher than 96%, indicating that the photochemical efficiency of PSI was not undermined when LHCI was substituted with LHCII as peripheral antenna moiety. Indeed, the PSIc–LHCII complex showed a reduction in the quantum yield of less than 0.01% in the 670–690 nm region compared with PSIc–LHCI.

Discussion

In this work we obtained a mutant with PSI complexes lacking LHCI complexes but with an increased association of LHCII. We therefore for the first time have been able to investigate the consequences of substituting LHCI by LHCII as an antenna system of PSI. The absence of LHCI subunits in the ΔLhca mutant induces an increase in LHCII binding to PSIc on state 2 induction, as a compensatory mechanism. The isolation of the PSIc–LHCII complex revealed the presence of a single LHCII trimer per PSI core based on carefully performed antenna cross-section measurements. The quantum efficiency of PSI in the presence of any combination of the LHC proteins investigated (LHCI, LHCII or LHCI plus LHCII

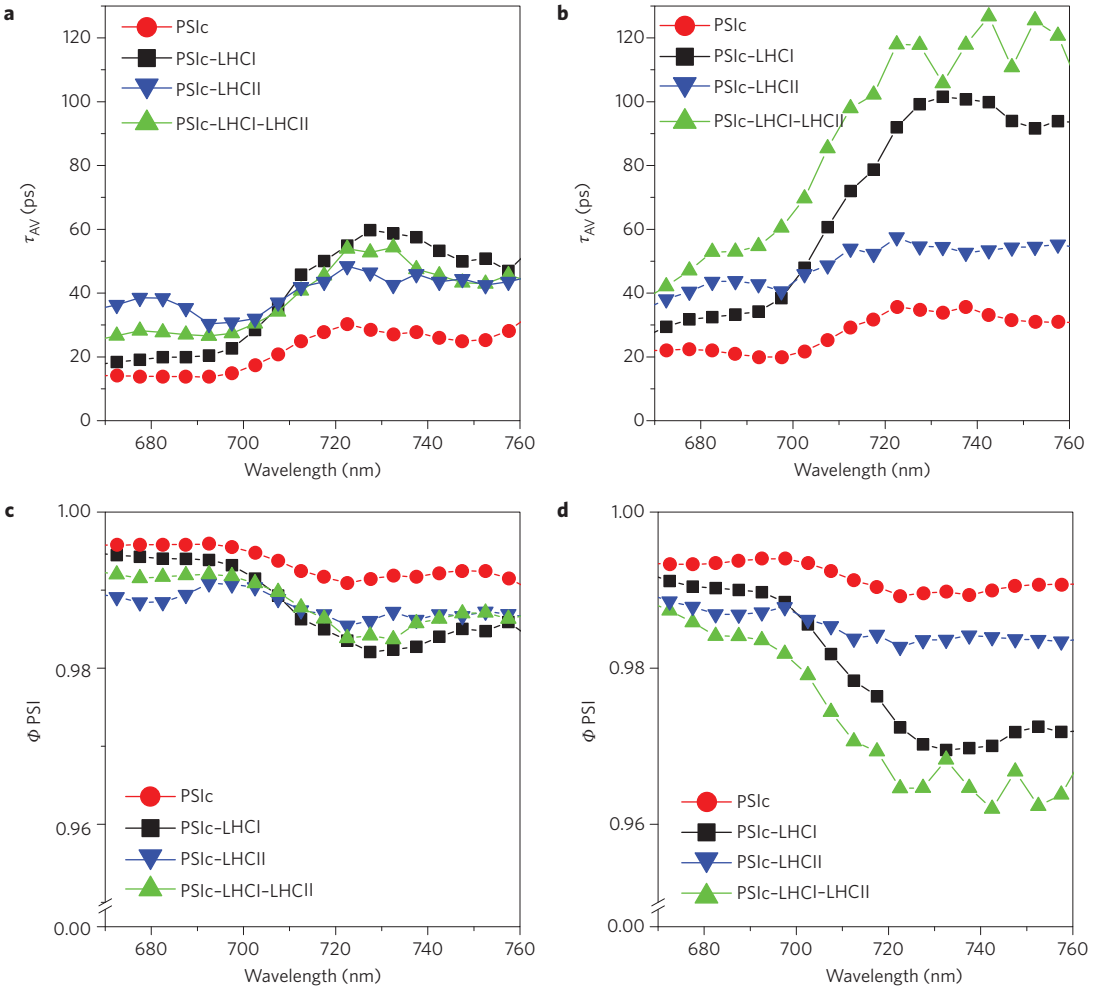

Figure 7 | Trapping time and quantum yield of PSI supercomplexes. a,**b**, Fluorescence average lifetime (τ_{AV}) was used to calculate the trapping time at the different wavelengths for PSIc, PSIc–LHCI, PSIc–LHCII and PSIc–LHCI–LHCII complexes upon excitation at 440 nm (**a**) and 475 nm (**b**). τ_{AV} was calculated using the time constants reported in Fig. 6 weighted by the amplitudes of the exponentials at each wavelength. **c**,**d**, Quantum yield (Φ) of PSI supercomplexes at each wavelength of emission, calculated as described in refs 25,26.

bound to the PSI core) was only slightly decreased compared with the bare PSI core and remained extremely high (>98%), in agreement with previous investigations of PSIc–LHCI vs. PSIc–LHCI–LHCII (refs 25,26,44). Here, we show that a PSIc–LHCII complex lacking LHCI is also characterized by very high quantum efficiency (Supplementary Table 5). LHCIs are thus not essential for excitation energy transfer from LHCII to PSIc, as demonstrated by the similar or even faster trapping time of PSIc–LHCII compared with PSIc–LHCI–LHCII (Supplementary Table 5). It is worth noting that a more evident reduction of trapping time would be expected in PSIc–LHCII, considering the reduced Chls content compared with PSIc–LHCI and PSIc–LHCI–LHCII: the discrepancy obtained could be ascribed to the very low amount of disconnected complexes present in PSIc–LHCII (<1%). Supplementary Fig. 6 indicates the presence of some disconnection in the PSIc–LHCII complex: on excitation at 475 nm, a very small population of PSIc and PSIc–LHCII still fluoresces on the nanosecond time scale, after more than 99% of the photoexcited population has already decayed. This small long-lived decay component was not resolved by global analysis because of its very low amplitude (<1%) but it can be ascribed to the presence of disconnected Chls or LHCIIs in PSIc and PSIc–LHCII samples, as revealed by 77 K fluorescence emission spectra (Supplementary Fig. 4). It should be noted that this long-lived component cannot be attributed to LHCI since the PSI samples were purified from *ΔLhca* plants and no traces of Lhca1-6 were detected in PSIc–LHCII (Supplementary Fig. 3). The detailed time-resolved fluorescence emission analysis presented here demonstrates that virtually all LHCII bound to PSI–LHCII in *ΔLhca* plants efficiently transfer energy to P700. It cannot be excluded, however, that the binding or energetic connection of some extra LHCII to PSI is impaired in *ΔLhca* plants; such an extra LHCII pool was indeed recently reported to be bound to PSI–LHCI in *A. thaliana* wild type, but was easily detached by digitonin treatment[45]. Our results clearly demonstrate that when LHCII was bound to PSI through digitonin-insensitive binding, the LHCI proteins were not essential for excitation energy transfer to the PSI reaction centre.

The main functional limitation of substituting LHCI by LHCII as an antenna system of PSI appears to be the reduction of the PSI absorption cross-section by 16% (Fig. 3 and Supplementary Table 3). Considering the 67% increase in PSI absorption cross-section on binding to LHCI, the contribution of each Lhca subunit can be roughly quantified at 16.5%. The substitution of the two Lhca1–4 and Lhca2–3 dimers by an LHCII trimer reduces the number of LHC proteins from four to three, and leads to the 16% reduction in absorption cross-section. The spectral form of the absorption loss upon substitution is evident in Fig. 3f. Reduced PSI excitation arising from the lower absorption cross-section of PSIc and PSIc–LHCII, compared with PSIc–LHCI or PSIc–LHCI–LHCII, has a consequence on the growth and wellness

of the *ΔLhca* mutant, as witnessed by the ~60% reduced growth reported in Fig. 1. Reduced fitness observed in the *ΔLhca* mutant is consistent with previous data reported for a mutant with antisense inhibition of the *Lhca4* gene only, resulting in reduction of LHCI proteins[46]. The reason why only LHCI adds four LHC proteins to PSI and LHCII binds as a trimer can be ascribed to the specific interactions involved in LHCI–PSIc binding, as in particular the Lhca1–PsaG, Lhca2–PsaJ, Lhca3–PsaA and Lhca4–PsaF interactions, which require specific charge pairing that is unlikely to be established by any LHCII monomer[2]. It is important to note that the substitution of LHCI by LHCII reduces the absorption at wavelengths above 700 nm (Fig. 4). When a plant grows under canopy conditions, the incident light is filtered by upper leaves, being enriched in far red light: in this conditions the presence of LHCI with its red forms is important to absorb at wavelengths above 700 nm, with a dramatic reduction of the intensity of the light absorbed by PSIc–LHCII compared with PSIc–LHCI on a filtering effect of only four leaves (Fig. 4). It should be considered that this effect is not only important under shaded canopy conditions but also within multicellular photosynthetic organisms that evolved red-shifted forms in their LHCI antenna moiety to fight competition by PSII antenna systems in the same organism or in others belonging to the same canopy.

Methods

Plant material and growth conditions. *Arabidopsis thaliana* T-DNA insertion mutant lines GT_5_2454 (N101690, insertion into the *Lhca* 2gene), SAIL_749_D03 (N876497, insertion into the *Lhca3* gene) and SALK_118680C (N679009, insertion into the *Lhca4* gene) were obtained from the NASC collection. Plants were grown in a phytotron for 5 weeks at 150 µmol photons m^{-2} s^{-1} (Epistar 35 mil Chip High Power LED, warm white LEDE-P20B-DW, Wayjun Tech.), 23 °C, 70% humidity, 8 h/16 h of day/night. Homozygous plants were identified by immunoblot for the lack of the corresponding gene product. The *kolhca2 kolhca3 kolhca4* (*ΔLhca*) genotype was obtained by crossing single mutant plants and selecting progeny. For RT–PCR, total RNA was isolated from 4-week-old plants following the Trizol protocol. Reverse transcription was performed using M-MLV reverse transcriptase with the oligo (dT) primer. 18S ribosomal RNA was chosen as an endogenous control. The transcripts were amplified from 25 ng of cDNA as a template and 2.5 units of TaqDNA polymerase using the followings cycles: 94 °C for 30 s, annealing at 55 °C for 30 s, 72 °C for 30 s, followed by a final extension step at 72 °C for 1 min. The primers used were as follows: 5′-TGGGTTAAGGCTCAGGAATG-3′and 5′-CAATTCCTCGAGCTTCTTGG-3′ for Lhca1 cDNA; 5′-TTCGGATTTGATCCTCTTGG-3′ and 5′-TTTATGCTCCGAATGACAATG-3′ for Lhca2 cDNA; 5′-CAAGGAGCCAACAGACCATT-3′ and 5′-TTCCCATAGATCCTGGGTTG-3′ for Lhca3 cDNA; 5′-CAGCCACAAAACTCGTTTCA-3′ and 5′-CATGGAGCTACAACGGTTCA-3′ for Lhca4 cDNA, and 5′-CAAATTTCTGCCCTATCAACTTTCGATGG-3′ and 5′-AATTTGCGCGCCTGCCTTCCTTT-3′ for 18S cDNA. To highlight the exponential phase, the amplification was stopped after 19, 23 and 27 cycles, and 5 µl for each gene was collected.

For excess light growth experiments, 2-week-old seedlings were transferred to either HL (1,000 µmol photons m^{-2} s^{-1}, 23 °C) or fluctuating light (alternations of 5 min at 150 µmol photons m^{-2} s^{-1} and 1 min at 1,000 µmol photons m^{-2} s^{-1}, 23 °C) during the 8 hour photoperiod. The growth rate was derived from the development of the rosette area by non-invasive image analysis and by measuring the fresh weight. All the growth trials were carried out using an LED light source (Epistar 35 mil Chip High Power LED, warm white LEDE-P20B-DW, Wayjun Tech.).

Isolation of PSI complexes. State 1 and state 2 were induced in the wild-type and mutant plants by exposure for 45 min to far red light (30 W incandescent bulbs filtered through a Lee Filters 027 Medium Red) or orange light (30 W warm white fluorescent lamps filtered through Lee Filters 105 Orange) respectively, as previously reported[20]. Thylakoid membranes were purified from treated leaves as described in previously[10] and solubilized by digitonin and α-dodecylmaltoside as reported[26]. Solubilized thylakoid membranes were loaded on Deriphat-PAGE native gel[31]. The bands corresponding to PSI-CORE (PSIc), PSI–LHCI (from now on named PSIc–LHCI), PSIc–LHCII and PSIc–LHCI–LHCII were eluted from acrylamide matrix using a solution with 10% glycerol, 10 mM HEPES pH 7.5 and 0.03% digitonin, protease inhibitors benzamidine (2 mM), PMSF (0.5 mM), ε-aminocaproic acid (5 mM). The experiments of state 1 and state 2 induction and purification of PSI supercomplexes were performed three times on independent biological material (at least 10 leaves for each genotype) obtaining

Pigment analysis. Pigments bound by the isolated PSI supercomplexes were extracted and analysed by fitting absorption spectra of pigment extracts fitted with chlorophyll and carotenoid absorption forms as previously described[47].

Absorption measurement. Absorption measurements of isolated PSI complexes were performed as described[47]. The spectra obtained were normalized to the same P700 content considering the Chl *a*/*b* ratio measured in the different samples, the different molar extinction coefficients of Chl *b* and Chl *a*, and the Chl/protein stoichiometry for PSIc, PSc–LHCI (refs 1,2) and LHCII (ref. 33). Absorption spectra were recorded for PSI supercomplexes purified in three different independent experiments obtaining reproducible results

Time-resolved fluorescence measurements. Time-resolved fluorescence measurements were performed using a femtosecond laser source and streak camera detection system, as described[40,48]. Briefly, samples were excited by ≅200 fs laser pulses at 440 or 475 nm, obtained from the second harmonic of a Ti:sapphire laser (Coherent Chamaleon Ultra II) and time-resolved fluorescent spectra were measured by a streak camera system (Hamamatsu C5680) with a time resolution of ≈3 ps. The laser power applied was 56 µW with a repetition rate of 80 MHz. Triplet-singlet annihilation could be excluded since no excitation power dependence of the decay kinetics was observed (Supplementary Fig. 11). Measurements were performed in an orthogonal geometry (beam waist in the focus of ~60 µm) and the sample was placed in a cooled cuvette at OD (absorbance) 0.06 cm^{-1}. The experiments for time-resolved fluorescence measurements were repeated three times on independent samples obtaining consistent results.

Global analysis. Global analysis of the time-resolved fluorescence data was performed using custom-coded Matlab software as previously described[49]. A confidence interval of 95% on amplitude and time constants was considered so that error bars could be calculated.

Photosystem II quantum yield and antenna size. The PSII quantum yield was determined as F_v/F_m, where F_m and F_v are respectively the maximum and variable fluorescence ($F_m - F_0$, where F_0 is the basal fluorescence of dark adapted samples) observed on exposure of intact leaf to a saturating pulse (6,000 µmol m^{-2} s^{-1}). Fluorescence measurements were performed with a DUAL PAM 100 (Walz) as previously described[30]. The PSII antenna size was measured following the kinetics of fluorescence emission in the millesecond time range upon illumination of DCMU-treated leaves as described[30].

P700 measurements. P700 measurements were performed using a time-resolved spectrophotometer (JTS-10 from BioLogic) following the decrease of absorption at 705 nm. For P700 measurements leaves were infiltrated with 50 µM DCMU, 50 µM dibromothymoquinone inhibiting linear and cyclic electron transport and 1 mM methyl-viologen to avoid limitation from the PSI electron acceptor. Maximum P700 oxidation per leaf surface was measured by absorption on illumination of leaves with an actinic orange light at 940 µmol m^{-2} s^{-1}). PSI antenna size was estimated from the ratio of P700 oxidation in limiting (12 µmol m^{-2} s^{-1}) vs. high light (940 µmol m^{-2} s^{-1})[50].

Received 29 January 2016; accepted 28 July 2016; published 26 August 2016

References

1. Qin, X., Suga, M., Kuang, T. & Shen, J. R. Photosynthesis. Structural basis for energy transfer pathways in the plant PSI-LHCI supercomplex. *Science* **348,** 989–995 (2015).
2. Mazor, Y., Borovikova, A. & Nelson, N. The structure of plant photosystem I super-complex at 2.8 Å resolution. *Elife* **4,** e07433 (2015).
3. Croce, R. & van Amerongen, H. Light-harvesting in photosystem I. *Photosynth. Res.* **116,** 153–166 (2013).
4. van Amerongen, H. & Croce, R. Light harvesting in photosystem II. *Photosynth. Res.* **116,** 251–263 (2013).
5. Jansson, S. A guide to the Lhc genes and their relatives in *Arabidopsis*. *Trends Plant Sci.* **4,** 236–240 (1999).
6. Ballottari, M., Girardon, J., Dall'Osto, L. & Bassi, R. Evolution and functional properties of Photosystem II light harvesting complexes in eukaryotes. *Biochim. Biophys. Acta* **1817,** 143–157 (2012).
7. Ballottari, M., Govoni, C., Caffarri, S. & Morosinotto, T. Stoichiometry of LHCI antenna polypeptides and characterization of gap and linker pigments in higher plants photosystem I. *Eur. J. Biochem.* **271,** 4659–4665 (2004).
8. Ben-Shem, A., Frolow, F. & Nelson, N. Crystal structure of plant photosystem I. *Nature* **426,** 630–635 (2003).
9. Amunts, A., Toporik, H., Borovikova, A. & Nelson, N. Structure determination and improved model of plant photosystem I. *J. Biol. Chem.* **285,** 3478–3486 (2010).
10. Ballottari, M., Dall'Osto, L., Morosinotto, T. & Bassi, R. Contrasting behavior of higher plant photosystem I and II antenna systems during acclimation. *J. Biol. Chem.* **282,** 8947–8958 (2007).

11. Williams, W. P. & Salamon, Z. Enhancement studies on algae and isolated chloroplasts. Part I.: Variability of photosynthetic enhancement in *Chlorella pyrenoidosa*. *Biochim. Biophys. Acta.* **430,** 282–299 (1976).
12. Hodges, M. & Barber, J. State 1-state 2 transitions in a unicellular green algae: analysis of in vivo chlorophyll fluorescence induction curves in the presence of 3-(3,4-dichlorophenyl)-1, 1-dimethylurea (DCMU). *Plant Physiol.* **72,** 1119–1122 (1983).
13. Wollman, F. A. State transitions reveal the dynamics and flexibility of the photosynthetic apparatus. *EMBO J.* **20,** 3623–3630 (2001).
14. Allen, J. F. Botany. State transitions–a question of balance. *Science* **299,** 1530–1532 (2003).
15. Grieco, M., Suorsa, M., Jajoo, A., Tikkanen, M. & Aro, E. M. Light-harvesting II antenna trimers connect energetically the entire photosynthetic machinery – including both photosystems II and I. *Biochim. Biophys. Acta* **1847,** 607–619 (2015).
16. Goldschmidt-Clermont, M. & Bassi, R. Sharing light between two photosystems: mechanism of state transitions. *Curr. Opin. Plant Biol.* **25,** 71–78 (2015).
17. Wientjes, E., Drop, B., Kouřil, R., Boekema, E. J. & Croce, R. During state 1 to state 2 transition in *Arabidopsis thaliana*, the photosystem II supercomplex gets phosphorylated but does not disassemble. *J. Biol. Chem.* **288,** 32821–6 (2013).
18. Bellafiore, S., Barneche, F., Peltier, G. & Rochaix, J. D. State transitions and light adaptation require chloroplast thylakoid protein kinase STN7. *Nature* **433,** 892–895 (2005).
19. Depège, N., Bellafiore, S. & Rochaix, J. D. Role of chloroplast protein kinase Stt7 in LHCII phosphorylation and state transition in *Chlamydomonas*. *Science* **299,** 1572–1575 (2003).
20. Pesaresi, P. *et al. Arabidopsis* STN7 kinase provides a link between short- and long-term photosynthetic acclimation. *Plant Cell* **21,** 2402–2423 (2009).
21. Pesaresi, P. *et al.* Optimizing photosynthesis under fluctuating light: the role of the *Arabidopsis* STN7 kinase. *Plant Signal. Behav.* **5,** 21–25 (2010).
22. Rochaix, J. D. *et al.* Protein kinases and phosphatases involved in the acclimation of the photosynthetic apparatus to a changing light environment. *Philos. Trans. R. Soc. Lond. B* **367,** 3466–3474 (2012).
23. Pribil, M., Pesaresi, P., Hertle, A., Barbato, R. & Leister, D. Role of plastid protein phosphatase TAP38 in LHCII dephosphorylation and thylakoid electron flow. *PLoS Biol.* **8,** e1000288 (2010).
24. Shapiguzov, A. *et al.* The PPH1 phosphatase is specifically involved in LHCII dephosphorylation and state transitions in *Arabidopsis*. *Proc. Natl Acad. Sci. USA* **107,** 4782–4787 (2010).
25. Wientjes, E., van Amerongen, H. & Croce, R. LHCII is an antenna of both photosystems after long-term acclimation. *Biochim. Biophys. Acta* **1827,** 420–426 (2013).
26. Galka, P. *et al.* Functional analyses of the plant photosystem I-light-harvesting complex II supercomplex reveal that light-harvesting complex II loosely bound to photosystem II is a very efficient antenna for photosystem I in state II. *Plant Cell* **24,** 2963–2978 (2012).
27. Akhtar, P. *et al.* Excitation energy transfer between light-harvesting complex II and photosystem I in reconstituted membranes. *Biochim. Biophys. Acta* **1857,** 462–472 (2016).
28. Wientjes, E., Oostergetel, G. T., Jansson, S., Boekema, E. J. & Croce, R. The role of Lhca complexes in the supramolecular organization of higher plant photosystem I. *J. Biol. Chem.* **284,** 7803–7810 (2009).
29. Morosinotto, T., Ballottari, M., Klimmek, F., Jansson, S. & Bassi, R. The association of the antenna system to photosystem I in higher plants. Cooperative interactions stabilize the supramolecular complex and enhance red-shifted spectral forms. *J. Biol. Chem.* **280,** 31050–31058 (2005).
30. Malkin, S., Armond, P. A., Mooney, H. A. & Fork, D. C. Photosystem II photosynthetic unit sizes from fluorescence induction in leaves: correlation to photosynthetic capacity. *Plant Physiol.* **67,** 570–579 (1981).
31. Järvi, S., Suorsa, M., Paakkarinen, V. & Aro, E. M. Optimized native gel systems for separation of thylakoid protein complexes: novel super- and mega-complexes. *Biochem. J.* **439,** 207–214 (2011).
32. Allen, J. F. Plastoquinone redox control of chloroplast thylakoid protein phosphorylation and distribution of excitation energy between photosystems: discovery, background, implications. *Photosynth. Res.* **73,** 139–148 (2002).
33. Liu, Z. *et al.* Crystal structure of spinach major light-harvesting complex at 2.72 A resolution. *Nature* **428,** 287–292 (2004).
34. Standfuss, J., Terwisscha van Scheltinga, A. C., Lamborghini, M. & Kühlbrandt, W. Mechanisms of photoprotection and nonphotochemical quenching in pea light-harvesting complex at 2.5 A resolution. *EMBO J.* **24,** 919–928 (2005).
35. Bassi, R., Croce, R., Cugini, D. & Sandonà, D. Mutational analysis of a higher plant antenna protein provides identification of chromophores bound into multiple sites. *Proc. Natl Acad. Sci. USA* **96,** 10056–10061 (1999).
36. Kouril, R. *et al.* Structural characterization of a complex of photosystem I and light-harvesting complex II of *Arabidopsis thaliana*. *Biochemistry* **44,** 10935–10940 (2005).
37. Morosinotto, T., Breton, J., Bassi, R. & Croce, R. The nature of a chlorophyll ligand in Lhca proteins determines the far red fluorescence emission typical of photosystem I. *J. Biol. Chem.* **278,** 49223–49229 (2003).
38. Rivadossi, A., Zucchelli, G., Garlaschi, F. M. & Jennings, R. C. The importance of PSI chlorophyll red forms in light-harvesting by leaves. *Photosynt. Res.* **60,** 209–215 (1999).
39. Laisk, A., Oja, V., Eichelmann, H. & Dall'Osto, L. Action spectra of photosystems II and I and quantum yield of photosynthesis in leaves in state 1. *Biochim. Biophys. Acta* **1837,** 315–325 (2014).
40. Ballottari, M. *et al.* Regulation of photosystem I light harvesting by zeaxanthin. *Proc. Natl Acad. Sci. USA* **111,** E2431–E2438 (2014).
41. Gobets, B. *et al.* Time-resolved fluorescence emission measurements of photosystem I particles of various cyanobacteria: a unified compartmental model. *Biophys. J.* **81,** 407–424 (2001).
42. Wientjes, E., van Stokkum, I. H., van Amerongen, H. & Croce, R. The role of the individual Lhcas in photosystem I excitation energy trapping. *Biophys. J.* **101,** 745–754 (2011).
43. Slavov, C., Ballottari, M., Morosinotto, T., Bassi, R. & Holzwarth, A. R. Trap-limited charge separation kinetics in higher plant photosystem I complexes. *Biophys. J.* **94,** 3601–3612 (2008).
44. Jennings, R. C., Zucchelli, G., Croce, R. & Garlaschi, F. M. The photochemical trapping rate from red spectral states in PSI-LHCI is determined by thermal activation of energy transfer to bulk chlorophylls. *Biochim. Biophys. Acta* **1557,** 91–98 (2003).
45. Benson, S. *et al.* An intact light harvesting complex I antenna system is required for complete state transitions in *Arabidopsis*. *Nat. Plants* **1,** 15176 (2015).
46. Ganeteg, U., Külheim, C., Andersson, J. & Jansson, S. Is each light-harvesting complex protein important for plant fitness? *Plant Physiol.* **134,** 502–509 (2004).
47. Ballottari, M., Mozzo, M., Croce, R., Morosinotto, T. & Bassi, R. Occupancy and functional architecture of the pigment binding sites of photosystem II antenna complex Lhcb5. *J. Biol. Chem.* **284,** 8103–8113 (2009).
48. Cesaratto, A. *et al.* Analysis of cadmium-based pigments with time-resolved photoluminescence. *Anal. Methods* **6,** 130–138 (2014).
49. van Stokkum, I. H., Larsen, D. S. & van Grondelle, R. Global and target analysis of time-resolved spectra. *Biochim. Biophys. Acta* **1657,** 82–104 (2004).
50. Bonente, G., Pippa, S., Castellano, S., Bassi, R. & Ballottari, M. Acclimation of *Chlamydomonas reinhardtii* to different growth irradiances. *J. Biol. Chem.* **287,** 5833–5847 (2012).

Acknowledgements

The work was financed by the Italian Ministry of Agriculture, Food and Forestry (MIPAAF) project HYDROBIO and by the Marie Curie Actions Initial Training Networks ACCLIPHOT (PITN-GA-2012-316427) and S2B (675006–SE2B) to R.B. G.C. acknowledges support from the European Research Council Advanced Grant STRATUS (ERC-2011-AdG No. 291198).

Author contributions

M.Ba., L.D. and R.B. conceived the work and designed the experiments. M.Br. and L.D. performed all the experiments for the isolation of the *ΔLhca* mutant, its physiological and biochemical characterization and purification of PSI complexes. M.Ba. performed all the experiments for the spectroscopic characterization of PSI complexes. C.D. and G.C. coordinated the time-resolved fluorescence analysis experiments. I.B., M.J.P.A. and C.D. contributed to the time-resolved fluorescence analysis experiments. I.B., M.J.P.A., D.V., G.C., M.Ba. and C.D. analysed the fluorescence decay results by global analysis. All of the authors contributed to writing the manuscript. All of the authors discussed the results and commented on the manuscript.

Additional information

Supplementary information is available for this paper. Reprints and permissions information is available at www.nature.com/reprints. Correspondence and requests for materials should be addressed to R.B.

Competing interests

The authors declare no competing financial interests.